Int. J. Electrochem. Sci., 13 **(2018)** 6027 – 6047, doi: 10.20964/2018.06.25

International Journal of
ELECTROCHEMICAL
SCIENCE
www.electrochemsci.org

Evaluation of Chloride Diffusion and Corrosion Resistance in Reinforced Concrete Using Internal Curing and Shrinkage Reducing Admixtures

F.J. Vázquez-Rodríguez[1,2,*], *A. Arato*[2], *Dora I. Martínez-Delgado*[2], *A. Guzmán*[2], *N. Elizondo-Villarreal*[3], *R. Puente-Ornelas*[2], *Edén Rodríguez*[2]

[1] Universidad Politécnica de Apodaca (UPAP); Av. Politécnica cruz con la carretera Miguel Alemán, km 24.5, Col. El Barretal, C.P. 66600, Apodaca, Nuevo León, México.
[2] Universidad Autónoma de Nuevo León, Facultad de Ingeniería Mecánica y Eléctrica, Centro de Investigación y Desarrollo Tecnológico, Av. Universidad S/N, Ciudad Universitaria, C.P.66455, San Nicolás de los Garza, Nuevo León, México.
[3] Universidad Autónoma de Nuevo León, Centro de Investigación en Ciencias Físico Matemáticas, San Nicolás de los Garza, N.L, 66451, México.
[*]E-mail: fcofimeuanl@gmail.com

Received: 1 February 2018 / *Accepted:* 9 March 2018 / *Published:* 10 May 2018

The properties of high-performance concretes obtained by the internal curing technique were studied in the fresh and hardened states. In some of the concrete mixtures, fine normal weight aggregates were replaced with lightweight aggregates (LWA) at 20 % vol. and ordinary portland cement was replaced by pulverized class F fly ash at 20 % by mass. Additionally, some mixtures were prepared including a shrinkage-reducing admixture, either as part of the mixing water or pre-soaked into the lightweight fine aggregates. The prepared concretes were subjected to degradation tests, such as accelerated carbonation and chloride ion deterioration. In addition, the reinforced concretes were analyzed through electrochemical corrosion tests with the linear polarization resistance technique. It was found that the internally cured concretes presented a mechanical resistance similar to those reported for the reference concretes (conventional concretes), but provided a higher resistance to carbonation, rapid penetration of chloride ions, and a lower chloride ion diffusion coefficient. The reinforcing steel structure in the internally cured concretes showed lower corrosion currents (I_{corr}) and corrosion potentials (E_{corr}) in comparison to the reference concretes. Therefore, the use of the internal curing technique in concretes with pre-soaking in either water or a solution of shrinkage-reducing admixture can be considered as a viable alternative to extend the service life of concrete structures in contact with harmful environments.

Keywords: Internal curing, Shrinkage reducing admixture, Corrosion, Concrete, Chloride diffusion.

1. INTRODUCTION

Nowadays, there are many problems related to the deterioration of reinforced concrete structures caused by corrosion phenomena resulting from the penetration of chloride ions and carbonation. This deterioration has promoted significant research in concrete technology [1–3]. The processing of concretes based on conventional methods, has been considered inadequate for the construction of buildings exposed to severe corrosion environments (in terms of durability).

The curing process for concretes is directly related to the evolution of mechanical resistance, cracking, and durability [4, 5]. The influence of internal curing (IC) with water has been proved to give beneficial results against desiccation, shrinkage, and cracking, since IC maintains a high humidity level throughout the concrete and thus, improving the hydration, in accordance with some physical and chemical phenomena. Up to 50 kg/m^3 of internal curing water may be required to mitigate shrinkage phenomenon [6–10].

It was reported the development of a concrete based on expansive cements by the addition of saturated LWA as internal curing agents to provide internal water to the concrete. In other words, they applied the autogenous curing concept to supply water internally into the matrix of the concrete to minimize shrinkage [11]. Additional research works, have found that the internal shrinkage in concretes is eliminated by the partial replacement of normal weight aggregates by LWA (around a 25 % replacement) [12].

The benefits of autogenous curing using LWA such as pumice have also been studied. The fraction of absorbed water available for the internal curing process using pumice is approximately 1, meaning 100 % efficiency [10–12]. It was claimed that the transport of water from pumice up to the interior of the cementitious matrix covered at least 4 mm from the source of the supplied water (the pumice surface) to the interior, enhancing the hydration process [13].

Moreover, an important parameter to determine the effectiveness of autogenous curing is the porosity of the LWA. The structure/size of pores and the percentage of porosity in the LWA in high-performance concretes have a positive impact due to the barrier effect on the densification of the cement-based matrix between the LWA and cementitious paste. Therefore, the high porosity of LWA is a useful tool for mitigating the autogenous shrinkage and diminishing the internal porosity of concretes. A positive effect related to durability and hydration is reached by the development of a suitable porosity percentage.

Newer technologies propose the use of viscosity modifier additives, for example, VERDiCT (viscosity enhancers reducing diffusion in concrete technology) [14, 15]. These additives modify the pore solution viscosity, thereby decreasing the penetration of aggressive agents into the cementitious matrix. VERDiCT technology has been applied to high-performance concrete exposed against conditions of accelerated deterioration, accelerated carbonation under laboratory conditions, and carbonation in a natural environment [1, 15]. As a result of this implementation, an improvement in the mechanical and durability properties using partial replacement of fly ash for ordinary portland cement (OPC) was found [1, 2]. Chloride penetration and carbonation are both critical concerns for assuring the durability of a field concrete [16-19].

On this basis, methods have been proposed to design internal curing concretes, since the internal curing method is a beneficial technique for concretes with low water/cement ratios and concretes, that are accompanied by chemical shrinkage and self-desiccation due to the hydration of portland cement and the low permeability of the hydrated microstructures [3, 4, 8, 15, 20].

Alternatively, a broad field of concrete technology is focused on water reduction to increase strength and improve durability. However, low workability and enhanced cracking at early ages due to contractions are also associated with lower water contents.

It was proposed to use chemical admixtures by the addition of cationic and anionic surfactants (HRWR) which improve the fluidity and workability of concretes [21, 22]. In 1983, one of the first research groups that developed shrinkage-reducing admixtures (SRA), established that SRA are typically organic compounds whose main purpose is to reduce the surface tension of the capillary pore solution to improve performance with respect to autogenous contraction and drying shrinkage [23]. Another research group studied the effects of SRA on the physical properties of normal concrete with 300 kg/m^3 cement contents, finding that the compressive strength may vary by ± 5 %, while some results showed a reduction of approximately 50 % to 60 % in drying shrinkage [24]. Also, it was studied the effects of SRA on high performance concretes (HPC) with silica fume. They concluded that after 28 d, the use of SRA increased the resistance by approximately 9 %. Besides, the SRA + silica fume combination contributed to a reduction of 52 % in drying shrinkage compared to mixtures with silica fume but without the addition of an SRA [25]. In 2010, the effect of hybrid curing methods using SRA and silica fume was studied. Their conclusions showed a decrease in contractions, as well as, improvements in mechanical resistance [26, 27]. Researchers claimed that SRA influence the reduction of the surface tension of the pore solution. In addition, SRA improves the performance against contractions for low *w/c* ratio mixtures. When the SRA dosage is increased by 1 %, 2 %, and 3% after a 60-day controlled cure, there is an improved performance against contractions with values of approximately 15 %, 30 %, and 48 %, respectively [28]. The effect of SRA on the autogenous contraction was studied, finding that SRA diminish the surface tension leading to a lower internal relative humidity. Also, he studied the reduction of water loss by evaporation when incorporating SRA. The conclusion showed that SRA reduces the water evaporation rate; thus, the concrete will remain more saturated, potentially increasing the degree of hydration of the cement [29]. This author also analyzed the performance of cement pastes with SRA at early ages, concluding that, in addition to reducing autogenous and drying shrinkage, SRAs increase both the pore solution viscosity (slowing diffusion) and the quantity of readily-freezable water in the pastes [30]. Recent studies have revealed that the use of SRA promotes the formation of portlandite over that of C-S-H gel, which further restricts the contraction. These admixtures features help to improve the properties in both the fresh and hardened states in concretes of high performance [31, 32].

As it was shown, the use of chemical admixtures and supplementary cementitious materials in synergy with the internal curing and viscosity modifiers are being considered by investigators as emergent technologies to improve the properties of concretes [33–45].

Although the corrosion rate of steel bars in concrete structures has been extensively studied by electrochemical techniques [46–73], the literature does not provide enough quantitative information regarding the corrosion rate of steel bar in internally cured concrete. A research group investigated and

predicted the service life of internally cured concretes, founding that the performance of high performance concrete structures can be substantially improved using LWA for internal curing, since it can reduce autogenous shrinkage, tensile stress development, chloride permeability, corrosion initiation, and corrosion propagation. However, these corrosion studies are not evaluated under electrochemical analytical techniques [74-77].

Considering the previously mentioned points, the present research work is a complement of a previous research [1, 56], whose aim is directed to investigate the physical and mechanical properties, as well as the corrosion resistance by an electrochemical method, of high-performance reinforced concretes created by the internal curing method to meet the requirements for aggressive environments.

2. EXPERIMENTAL PROCEDURES

2.1. Materials and specimen preparation

The raw materials used are commercially available products, such as OPC with a cumulative median diameter (50 % pass particle size), d_{50} of 30 µm, class F fly ash (PFA) [78] with a d_{50} of 75 µm, fine aggregates of normal weight (FLA), coarse aggregates of normal weight (CA) and a lightweight pumice aggregate (LWA).

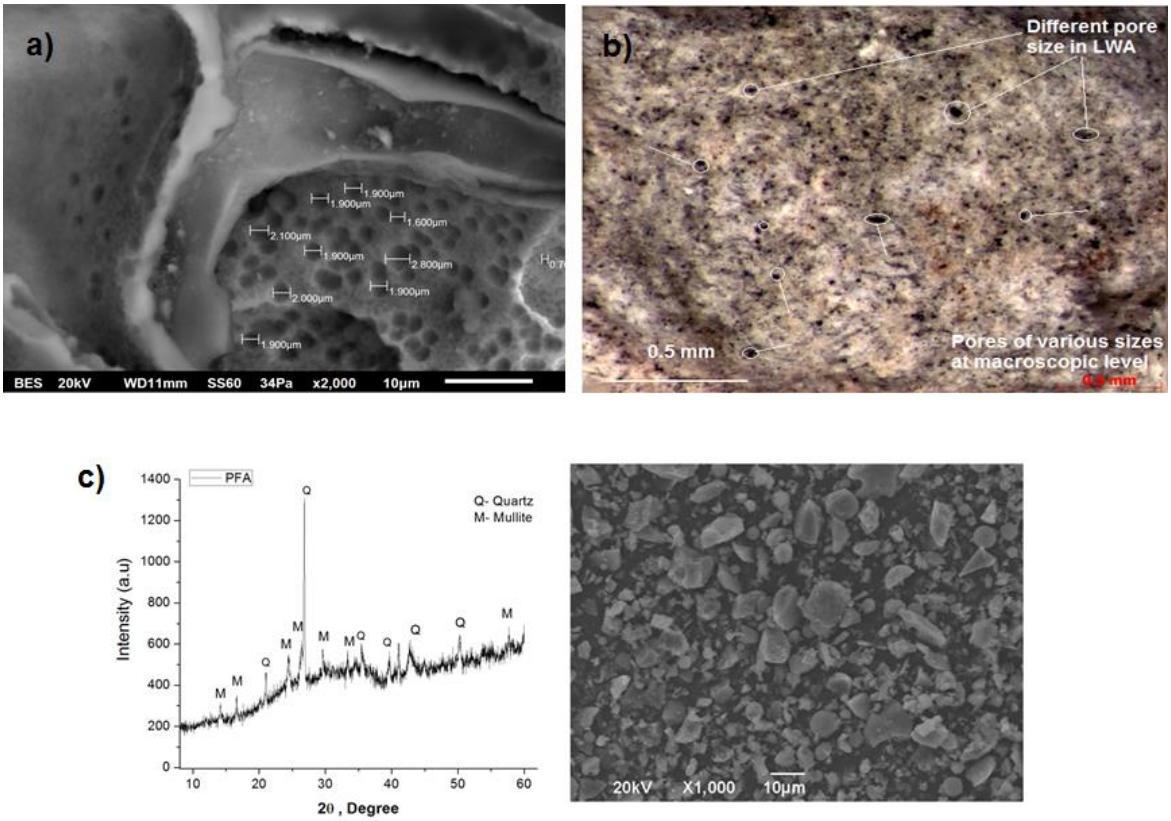

Figure 1. (a) SEM image of the morphology and the internal pores distribution of lightweight aggregate (LWA), (b) Optical microscopy image of LWA, (c) X-ray diffraction and SEM image of a morphology of fly ash.

LWA and PFA were characterized by optical and electronic microscopy using a JEOL JSM-6490LV microscope. Figures 1(a) and (b) show the internal porosity and morphology of the LWA. From this analysis, pores with diameters ranging from 0.70 μm to 2.8 μm, with an average pore diameter of about 2 μm were registered. Figure 1(c) shows the morphology and composition of the PFA.

Additives, such as a commercial full-range water reducing admixture (superplasticizer), and a commercial shrinkage-reducing admixture (SRA) were used.

Table 1. Chemical composition of the raw material obtained by X-ray fluorescence (wt. %).

Raw material	Na_2O	MgO	Al_2O_3	SiO_2	P_2O_5	K_2O	CaO	Cr_2O_3	Fe_2O_3
LWA	1.71	0.43	14.36	72	0.04	0.05	2.74	0.06	3.71
FA	-	1.06	0.42	1.6	-	0.01	97	-	0.01
PFA	0.64	0.84	25.01	63.8	0.02	0.01	2.29	0.05	4.99
OPC	0.37	1.68	5.84	20.7	0.12	0.01	65.8	0.07	2.35

Table 2. Mixture proportions of the concretes (kg/m^3) (Saturated Surface Dry).

Mixture	R1	R2	IC1	IC2	IC3	IC4
OPC	422	336	421	424	423	338
PFA	-	84	-	-	-	85
Water	168	167	168	166	168	168
CA	789	781	788	788	791	786
FA	980	986	800	783	786	781
LWA	-	-	117	117	117	117
SRA	-	-	0.0	6.36	19.5	19.3
HRWRA	1.13	1.13	1.13	1.13	1.13	1.13
w/cm	0.40	0.40	0.40	0.40	0.40	0.40

Table 1 shows the chemical composition of the raw material, obtained by X-ray fluorescence using an X EPSILON 3-XL. A *w/c* (water/cement) ratio of 0.4 by mass was used in the production of the high-performance concretes with a cement content of approximately 400 kg/m^3. Concretes were fabricated in a mixer with a capacity of 90 L. Tables 2 and 3 show the mixture proportions of the concretes and their compositions respectively. After mixing, physical properties in a fresh state were evaluated. Tests were performed on concretes in a fresh state according to their volumetric weight

(kg/m^3) (ASTM C138) [79], assurance of slump (ASTM C143) [80] and air content (ASTM C173) [81].

Table 3. Composition of concretes (mix proportions).

Description of elaborated concretes	
R1	Concretes with normal weight aggregates, ordinary portland cement, water and High-Range Water-Reducing Admixture (HRWRA).
R2	Concrete with normal weight aggregates, partial substitution of ordinary portland cement by pulverized fly ash at 20%, water, and High-Range Water-Reducing Admixture (HRWRA).
IC1	R1 concrete modified with a partial substitution of 20% of lightweight aggregate (LWA) by a fine aggregate of normal weight FLA.
IC2	IC1 concrete provisioned with Shrinkage-Reducing Admixture (SRA) in the mixing process.
IC3	IC2 concrete with the lightweight aggregates (LWA) saturated with Shrinkage-Reducing Admixture (SRA).
IC4	Concrete with normal weight aggregates, partial substitution of ordinary portland cement by pulverized fly ash at 20%, water, substitution of the FLA by LWA saturated with SRA.

After these tests, the fresh concrete was poured into cylindrical metal molds with dimensions of 75 mm × 150 mm, and 100 mm × 200 mm. During the first hour, the samples were maintained in an environment at 25 °C and 90 % RH.

Next, the samples were demolded after 24 h and placed to cure in water for 14 d. Each sample had a steel bar (composed mainly by ferrite and perlite phases) with a length of 150 mm and a diameter of 6.4 mm embedded in its center. The steel bars were characterized in accordance with the ASTM A370 standard [82]. The yield strength obtained was 361 MPa and the rupture strength was 555 MPa. The steel bars were cleaned with acetone prior to placement in the concrete. A 60 mm long exposure zone was established, which corresponds to the area that was embedded within the concrete. The rest of the bar was coated with corrosion resistant epoxy paint.

2.2. Mechanical testing (compressive strength and modulus of elasticity)

The compressive resistance was evaluated on cylindrical samples with dimensions of 100 mm x 200 mm at 14 d, 28 d, 90 d, and 180 d in accordance with the ASTM C39 standard [83]. An ELE International mechanical test machine was used to perform the compressive tests. The loading

parameter during the compression test was 0.5 MPa/s. For each aging time, three samples were examined, and the median value was reported.

In addition, the modulus of elasticity was evaluated on cylindrical samples with dimensions of 100 mm × 200 mm at 14 d, 28 d, 90 d, and 180 d in accordance with the ASTM C469 standard [84].

2.3. Water absorption

Water absorption measurements were evaluated according to the ASTM C642 standard (the standard test method for density, absorption and voids in hardened concretes) to estimate the permeability caused by the interconnected porosity of porous granular materials, which can be responsible for concrete degradation due to the infiltration of aggressive agents [85]. The water absorption evaluation was carried out in samples cured for 28 d and 90 d.

2.4. Rapid chloride permeability

Using a Nordtest BUILD 492 equipment, the chloride permeability of the concretes was evaluated following the ASTM C1202 standard (the standard test method for electrical indication of concrete's ability to resist chloride ion penetration) [86]. Cylindrical shape samples of 100 mm diameter elaborated according to the compositions given in Table 3, were cut into sections with a thickness of 50 mm. The secctions were then coated with a setting epoxy resin and put into voltage cells in order to calculate the electric charge that passed through them. The cathodic terminal was connected to a 3 % NaCl solution and the anodic area to a 0.3 M NaOH solution. A 60 VDC potential difference was applied between the two sections during the measurement. The voltage and resistance between the cells were recorded every 30 min for up to 6 h. The current of the cell was calculated from the voltage measurements and the total passed charge was calculated using Eq. (1) as:

$$Q = 900\ X\ [I_o + 2I_{30} + 2I_{60} + \ldots + 2I_{330} + I_{360}] \quad (1)$$

Where Q is the total charge passed through the sliced specimen (C) and I is the current (A) at n minutes after the voltage is applied. A cumulative charge passed a value of less than 2000 C is characterized as low chloride permeability, 2000 C to 4000 C is the medium level, and higher than 4000 C is defined as high chloride permeability. The penetration depth was measured after the test was finished. The sliced samples were split into two sections, and a 0.1 M $AgNO_3$ solution was sprayed onto the fracture surfaces. The penetrated zone was indicated by the change in color (to a brownish tone) of the fracture surfaces. For each concrete type, the total charge passed was measured from at least two sets of sliced samples and the penetration depth from 10 measuring points on each fracture surface.

2.5. Chloride diffusion

The chloride content and chloride diffusion coefficient of the concretes were evaluated using 100 mm × 200 mm cylindrical samples. After 14 d of curing, the cylinders were cut into sections with a thickness of 50 mm, and two samples of each concrete type were settled in a container with a NaCl

solution prepared according to the ASTM C1556 standard [87]. The samples remained immersed in the exposure solution for 60 d. The chloride ingress is shown in figure 2a-d, where the silver nitrate sprayed on the concrete specimen, reveals the area without chlorides (brown area). After this, pulverized concrete samples were collected at depth increments from 1 to 16 mm, in accordance to the ASTM C1556 standard. Figure 2e shows the procedure for obtaining powder to evaluate the chloride diffusion coefficient in concretes. The chloride contents of the powder samples were measured using an 848 Titrino plus (Metrohm). An accurately weighted 3g sample was dissolved in 35 ml of distilled water and, after that, 0.9 ml of concentrated nitric acid was added. Finally, the whole sample was precisely measured.

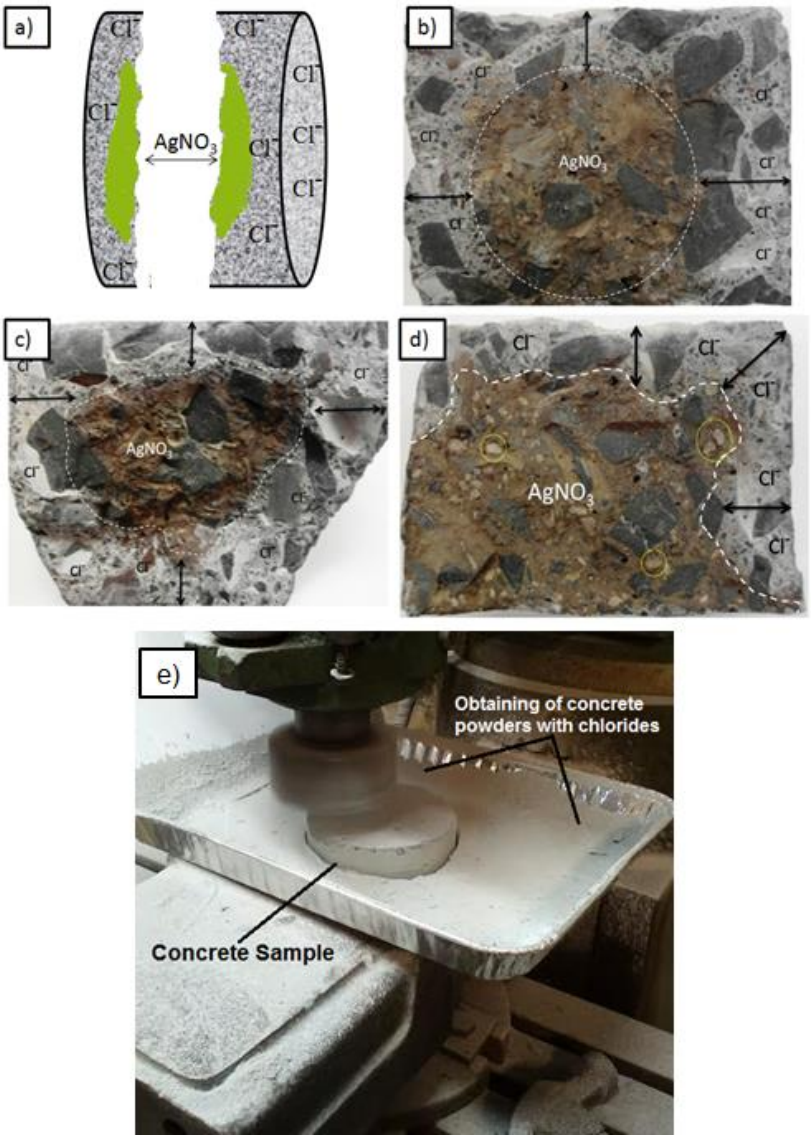

Figure 2. (a) Test to determine the diffusion coefficient of chlorides in concretes. Schematic model of the specimen exposed to chloride ions, (b) Uniform diffusion of chloride ions IC3 concrete mixture, (c) High concentration of chloride ions in R2 concrete mixture, (d) Lower penetration of chloride ions IC4 concrete mixture, (e) Test to determine the diffusion coefficient of chlorides in concretes.

The chloride ions reacted with the acid of the liquid in an electrochemical reaction. An electrode was inserted into the liquid and the electrochemical reaction was quantified. The percentage of chloride was displayed directly on the LCD readout. The chloride diffusion coefficient for each sample was determined by fitting the data obtained in the chloride profile analysis to Fick's second law of diffusion.

Fick's second law of diffusion is best represented by a differential equation that describes how the concentration of diffusing species varies with time in a specific medium. For a one-dimensional diffusion phenomenon, the differential equation is as it follows:

$$\frac{\partial \mathrm{C}\,(\mathrm{x,t})}{\partial \mathrm{t}} = \mathrm{D}_0 \frac{\partial^2 \mathrm{C}\,(\mathrm{x,t})}{\partial \mathrm{x}^2} \quad (2)$$

From a dimensional analysis, it can be shown that the diffusion coefficient, D_0, has units of length^2/time. The chloride penetration distance is measured in mm and exposure time in terms of years.

If it is assumed that there is one-dimensional diffusion and that the chloride ion content at the surface is constant, a solution to Fick´s second law is as follows:

$$C(x,t) = \mathrm{Cs} - (\mathrm{Cs} - \mathrm{Ci}).erf\left(\frac{X}{\sqrt{4.\mathrm{D}_0.t}}\right) \quad (3)$$

where *C(*x, t) is the chloride ion concentration at a depth, x, in mm from the exposed surface for an elapsed time, t, in years, since the start of chloride exposure, Cs is the chloride concentration at the surface, expressed as a % of concrete mass, Ci is the initial (or background) chloride concentration of the concrete, expressed as a % of concrete mass, erf is the error function (a special function related to the integral of a normal probability function), and D_0 is the chloride diffusion coefficient in mm^2/year.

The experimental procedure for determining the chloride diffusion coefficient was taken from ASTM C1556 and some similar research works described elsewhere[87-89].

2.6. Accelerated carbonation test

The accelerated carbonation test was determined at 25 °C and 10 % RH with a 4 % CO_2 concentration in the carbonation chamber. The concrete samples (70 mm × 50 mm) were cut into sections of 30 mm of thickness and a 1 % phenolphthalein solution was sprayed onto the fracture surfaces. After 1 min or 2 min, when the sample turned to a magenta color tone, the thickness of the colorless layer was measured and the average value of the measurements was then determined. The carbonated depth was measured, as a color change after 14 d, 28 d, 90 d, and 180 d of carbonation exposure in ten surfaces for each concrete type.

2.7. Corrosion current density (I_{corr}) from linear polarization resistance (LPR)

The potentiostatic linear polarization resistance (LPR) test method has been used to assess the corrosion rate in steel bar. Negligible corrosion is represented by a corrosion current density (I_{corr})

value of less than 0.1 μA/cm^2, while a value greater than 0.3 μA/cm^2 is correlated with active corrosion. The corrosion current density was measured using the direct current LPR method with a lower potential. The resistance to polarization (R_p) was evaluated by conducting a linear polarization scan in the range of ± 25 mV of the open circuit potential at a scan rate of 0.2 mV/s.

The Rp was calculated using the Stern-Geary formula (see: Eq. 4).

$$R_p = \beta/I_{corr} \quad (4)$$

Where β is the proportionality constant for the particular corrosion system (the value of β was taken as 26 mV, considering steel in active conditions) and I_{corr} is the corrosion current density (μAcm^2)

β was determined from the anodic and cathodic slopes of a Tafel plot (β_a and β_c), respectively (see Eq. 5) [90]:

$$\beta=(\beta_a \cdot \beta_c)/((2.303(\beta_a+\beta_c)) \quad (5)$$

Corrosion current density, I_{corr}, is the current per unit area at the corrosion potential. I_{corr} can be used to calculate corrosion rate. If Eq. 4 is substituted in Eq. 5, corrosion current density in terms of polarization resistance can be calculated as (see Eq. 6):

$$I_{corr}=(\beta_a \cdot \beta_c)/((2.303 \cdot R_p(\beta_a+\beta_c)) \quad (6)$$

Thus, the corrosion current can be used to calculate the corrosion rate using (Eq. 7) as:

$$Corrosion\ rate\ (mpy) = \frac{0.13\ Icorr\ (\text{Eq wt})}{d} \quad (7)$$

Where I_{corr} is corrosion current density, (A/cm^2), d, the density of the corroding metal (g/cm^3) and Eqwt, is the equivalent weight of the corroding metal in grams. [91, 92]

For the LPR measurements, an electrochemical cell with three electrodes was used, with a working electrode (steel bar embedded in concrete), a reference electrode (electrode of saturated calomel (SCE), and an auxiliary electrode (a platinum counter-electrode). A potential in the interval of -20 mV to +20 mV was applied to the cell. A potentiostat/galvanostat (Autolab Instrument PG5 EV) was used to polarize the steel at a rate of 0.2 mV/s. The process of wet-dry cycling consisted of 11 cycles. In each cycle, the samples were exposed to chlorides by 3-d partial immersion in a 35 g/L NaCl solution, followed by 4 d drying period at 40ºC in a forced ventilation oven. After 20 weeks of exposure, the total chloride concentration near to the steel-concrete interface (around 1 cm of steel) was higher than permitted (4 % by mass of cement). Figure 3 shows the electrochemical measurement procedure. Tafel constants were utilized in the calculation of the corrosion current density.

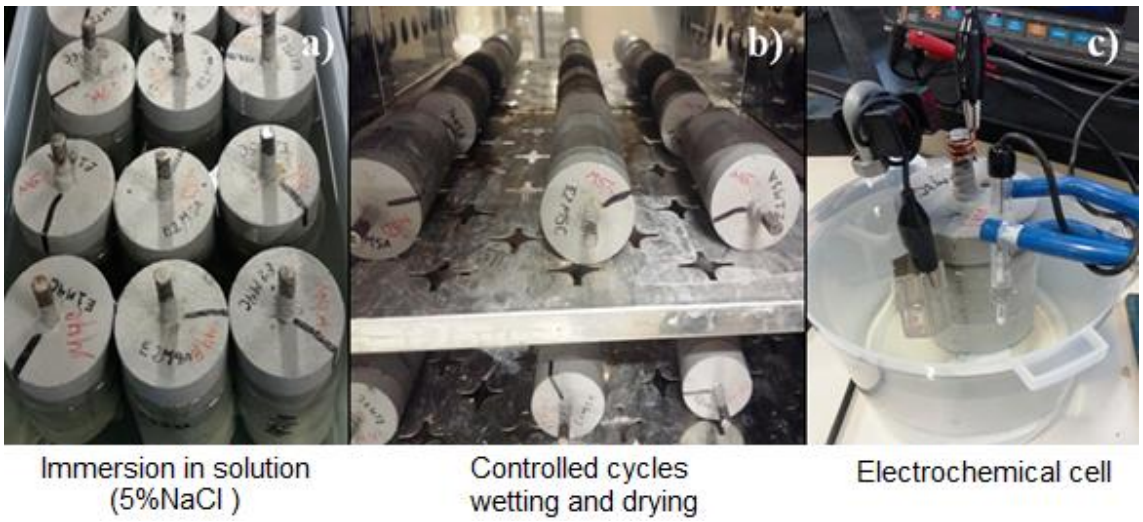

Figure 3. The electrochemical measurements procedure.

3. RESULTS AND DISCUSSION

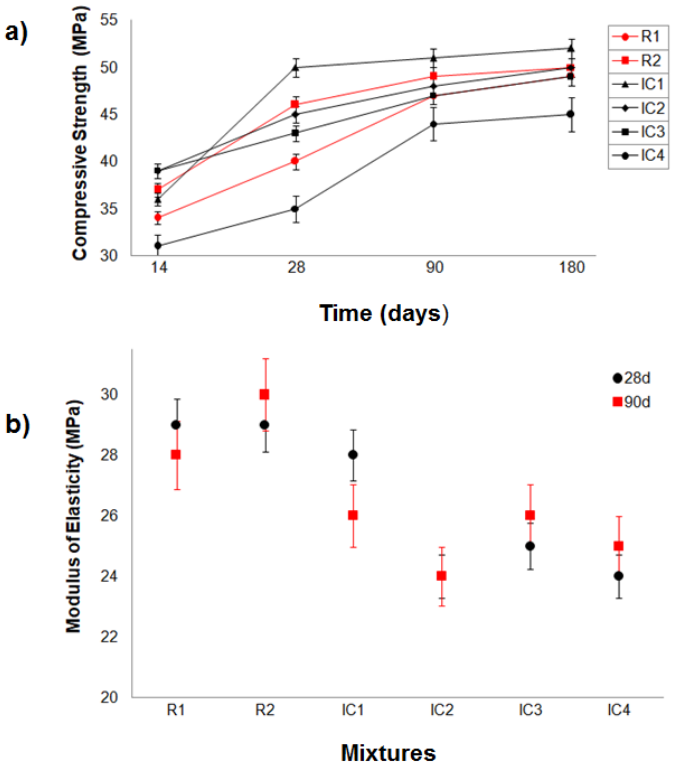

Figure 4. Mechanical properties of the analyzed concretes. (a) Compressive resistance, (b) Modulus of elasticity.

Table 4 shows the properties of the elaborated concretes in a fresh state (volumetric unit weight, the slump, and air content). The volumetric weight is around 2260 kg/m^3 to 2410 kg/m^3, while the slump ranges between 130 mm and 190 mm. Finally, the air content was determined with values of around 2.25 % to 2.50 %.

The mechanical properties of the analyzed concretes can be observed in Figure 4. The results of the compression tests carried out in the laboratory after curing periods of 14 d, 28 d, 90 d, and 180 d are also shown in Figure 4(a).

Table 4. Results of physical properties of the tested concretes in a fresh state.

Mixture	ASTM C138 Volumetric Weight (kg/m^3)	ASTM C143 Slump (mm)	ASTM C173 Air content (%)
R1	2,350	160	2.50
R2	2,410	140	2.25
IC1	2,310	130	2.25
IC2	2,290	160	2.50
IC3	2,310	140	2.25
IC4	2,260	190	2.50

After 14 d of curing, IC2 and IC3 obtained the highest compressive strength (39 MPa). This value represents mechanical improvements of 5.4 % and 14.7 % based on the values found for R2 (37 MPa) and R1 (34 MPa), respectively. IC1 has a higher compressive strength than R1 by around 5.9 %; however, its resistance is lower than R2 by around 2.7 %. The compressive strength of IC4 after 14 d of curing was the lowest with a strength value of 31 MPa.

IC1 reached the highest compressive strength (50 MPa) of all proposed formulations after 28 d of curing. Comparing to the reported values for R1 (40 MPa) and R2 (46 MPa), IC1 obtained mechanical improvements of 25 % and 8.6 % respectively. The IC2 and IC3 formulations registered improvements in compressive strength percentages of 12.5 % and 7.5 % respectively, if we compare them to the R1 formulation. However, according to the values obtained by R2, IC2, and IC3 presented lower compressive strengths by about 2.17 % and 6.52 %.

After 90 d of curing, IC1 showed the highest mechanical strength (51 MPa), followed by R2 (49 MPa) and IC2 (48 MPa). The R1 and IC3 formulations showed a lower compressive strength value of 47 MPa, while it is clearly observed that IC4 presented the lowest mechanical strength at 90 d of curing (44 MPa).

After 180 days of curing, IC1 again reached the highest compressive strength (52 MPa). This value resulted in mechanical improvements of 6.12 % and 4 % compared to those for R1 (49 MPa) and R2 (50 MPa). IC2 obtained the same compressive strength value as R2 (50 MPa) and a strength improvement of 2.04 % compared to R1. Finally, IC4 showed a resistance value of 45 MPa, which was again the weakest of all tested formulations.

In general, the compressive strength results showed that the strength of IC1, which was made of porous LWA pre-soaked in water, was superior to those of R1 and R2. This formulation's strengths were also higher than those of IC2, IC3, and IC4, the latter being formulated with PFA. This compressive strength improvement may be due to an internal curing effect, since in porous LWA, moisture transfers from the aggregates to the cement paste, via a porous network and further stimulates a hydration reaction after a period of time [93]. In addition, the bond between the aggregates and the matrix is stronger in the case of LWA than in normal concrete. Cement paste penetrates into the

aggregates because of their porous nature. Thus, there is a negligible interfacial transition zone between the aggregates and the matrix [94]. These phenomena increase strength. Figure 4(b) shows the modulus of elasticity results. From the analysis, it was found that the formulations with internal curing (IC1, IC2, IC3, and IC4) show a lower elastic modulus range than the reference concretes (R1 and R2) at both 28 d and 90 d. This phenomenon can be attributed to the lower density of the lightweight fine aggregates, as it is well known that the modulus of lightweight concrete is generally less than that of a comparable concrete prepared with normal weight aggregates.

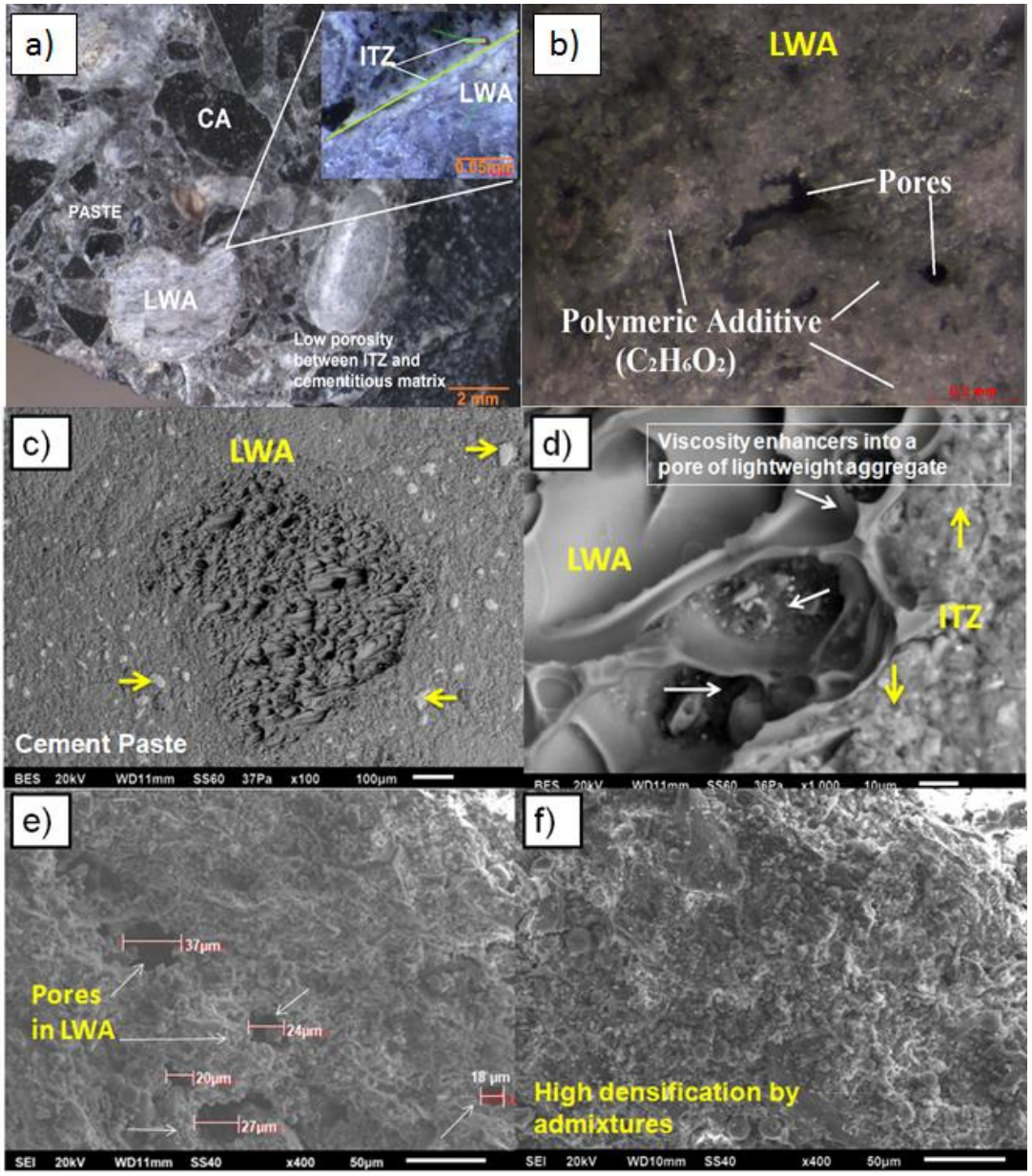

Figure 5. SEM image of the IC4 concrete microstructure. (a) The internal curing effect of the aggregates in the cementitious matrix and the interfacial zone in the concrete are observed, (b) Shrinkage reducing additive supply by LWA, (c) LWA inside the cementitious matrix, (d) Desorption SRA Interface LWA / paste, (e) Large pores in the LWA, (f) Effect of SRA and FA on the densification of concrete.

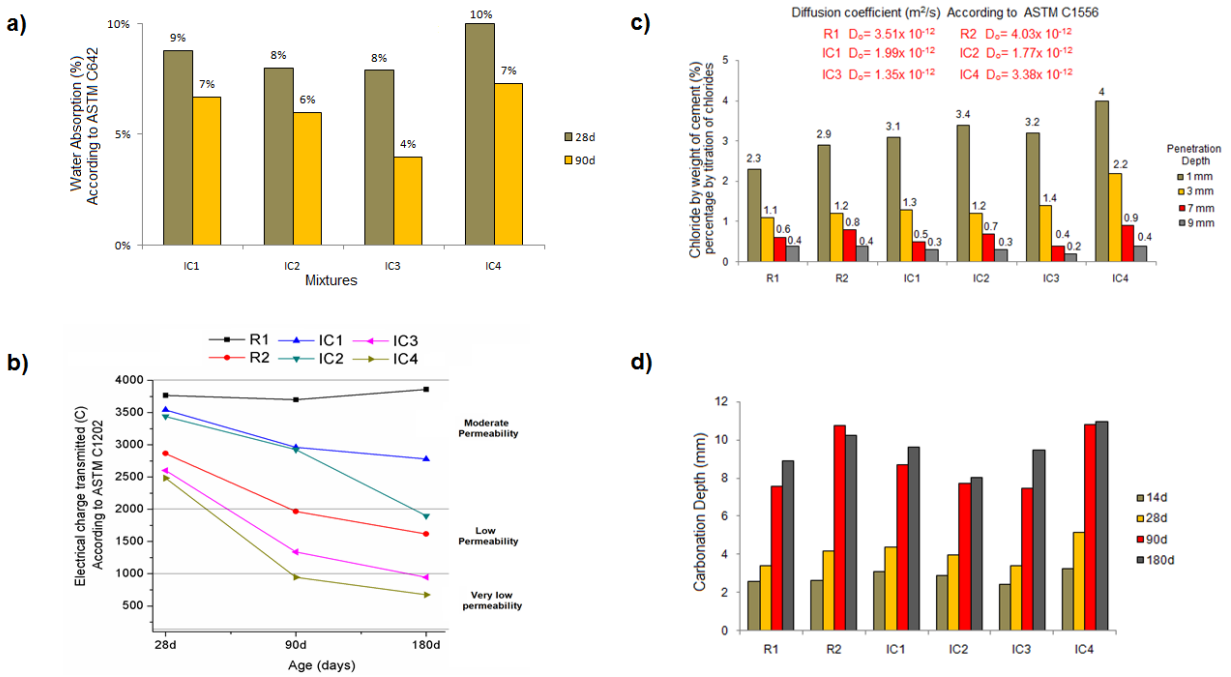

Figure 6. Accelerated durability results of the tested concretes. (a) Water absorption capacity, (b) Rapid chloride permeability, (c) Chloride diffusion coefficient, (d) Carbonation depth.

To corroborate this phenomenon, a petrographic analysis using a ZEISS Axio Zoom V16 optical microscope was completed. Figure 5(a) and 5(b) show the IC4 microstructure, where a higher densification in the interfacial zone between LWA and the cement paste is observed. This microstructural characteristic is probably due to the LWA desorption effect and perhaps the SRA chemical interaction with the C-S-H gel of the OPC. A homogenous distribution of LWA throughout the cementitious matrix and the physical interaction between LWA with the aggregates of normal weight CA and FLA were observed in the figure 5(c-f).

The accelerated durability results of the tested concretes are shown in Figure 6. Figure 6(a) shows the results of the water absorption test only in mixtures with internal curing. After 28 d of curing, IC2 and IC3 obtained the lowest water absorption (8 %), while IC1 and IC4 obtained slightly higher values corresponding to 9 % and 10 %, respectively. After 90 d of curing, IC3 gave the lowest value (4 %), followed by IC2 with a water absorption of 6 %. IC1 and IC4 registered the same water absorption value (7 %). This behavior indicates that the cementitious matrices of the IC3 and IC2 concretes are denser than those for IC1 and IC4, which diminishes the infiltration of harmful agents.

The rapid chloride permeability results are shown in Figure 6(b). According to ASTM C1202, concretes with transmitted electrical charges ranging from 2000 C to 4000 C can be considered as moderate permeability. Taking into account the above criteria, at an aging of 28 d, in general, all the concretes proposed are in this range; however, IC4 registered the lowest permeability (2400 C). After 90 d of curing, R1 and IC2 moved to the low permeability zone (2000 C to 1000 C) with charges of 1965 C and 1300 C, respectively. Once again, IC4 registered the lowest charge with 945 C. This value has placed this in the very low permeability zone (1000 C to 0 C), while R2, IC1, and IC3 stayed in the moderate permeability zone. Finally, after aging 180 d, only IC4 and IC2 resulted in a very low

permeability (945 C and 673 C, respectively). R1, R2, and IC3 are in the low permeability zone. IC1 exhibited the poorest behavior against chloride ion penetration (2779 C) possibly due to the absence of SRA in this mixture. The concretes that showed better behavior were IC4, IC2, and R1. In the case of IC4 and IC2, where LWA with SRA additions were used, the synergic effect of LWA and SRA provides a good performance as the release of the SRA solution from the LWA into the surrounding cement matrix produces a pore solution of higher viscosity that will slow diffusion and electrical conduction [15].

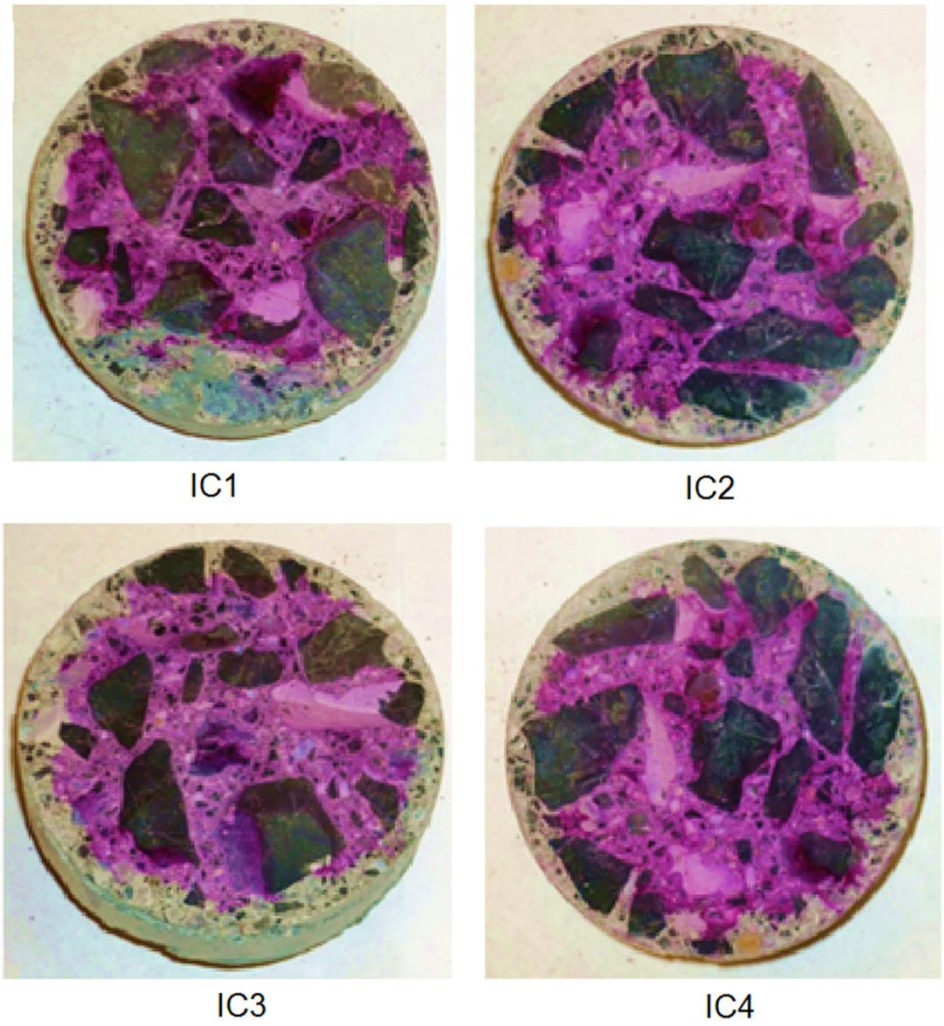

Figure 7. Carbonation profile of the internally cured concretes.

The calculated chloride diffusion coefficients of the concretes are presented in Figure 6(c), along with the measured chloride ion profiles as a function of penetration depth. For the R1 concrete, the chloride ion diffusion coefficient is 3.51 x 10^{-12} m^2/s, while for R2, the chloride coefficient is 4.03 x 10^{-12} m^2/s. In decreasing order, the diffusion coefficients of the IC concretes mixtures are 3.39 x 10^{-12}, 2.0 x 10^{-12}, 1.77 x 10^{-12} and 1.36 x 10^{-12} m^2/s for IC4, IC1, IC2, and IC3, respectively. The value of D_0 of IC3 is decreased by 61 % from the R1 concrete and 66 % from the R2 concretes after a 60 d exposure. For IC2, the value of D_0 decreased by 49 % from the R1 concretes and 56 % from the R2

concretes. For IC1, the value of D_0 decreased by 43 % from the R1 concretes and 50 % from the R2 concretes. For IC4, the value of D_0 decreased by 3.4 % from the R1 concretes and 16 % from the R2 concretes. It is clear that the LWA and SRA additions influence the reduction of chloride ion diffusivity, as observed in a previous study [56, 95].

Figure 6(d) shows the measured carbonation depths, which generally increased with increasing exposure time. In the test results, the carbonation depth was lower in the IC2, IC3, and R1 concretes, meanwhile higher carbonation depths were observed in the IC1, R2, and IC4 concretes. The results indicate that in concretes, where LWA with the addition of SRA were used, as in the case of the IC2 and IC3 concretes, better resistance against carbonation was observed. In contrast, greater carbonation depths were observed in the R2 and IC4 concretes that contained fly ash, as these mixtures will contain less calcium hydroxide (following its pozzolanic reaction with the fly ash) to react with the carbon dioxide [1]. In a complementary study, the carbonation level in the concretes created using the internal curing technique was measured by the phenolphthalein test. The carbonation profile in Figure 7 shows a lower carbonation in the IC2 and IC4 samples. The magenta color of the samples corresponds to the non-carbonated zone of the concretes.

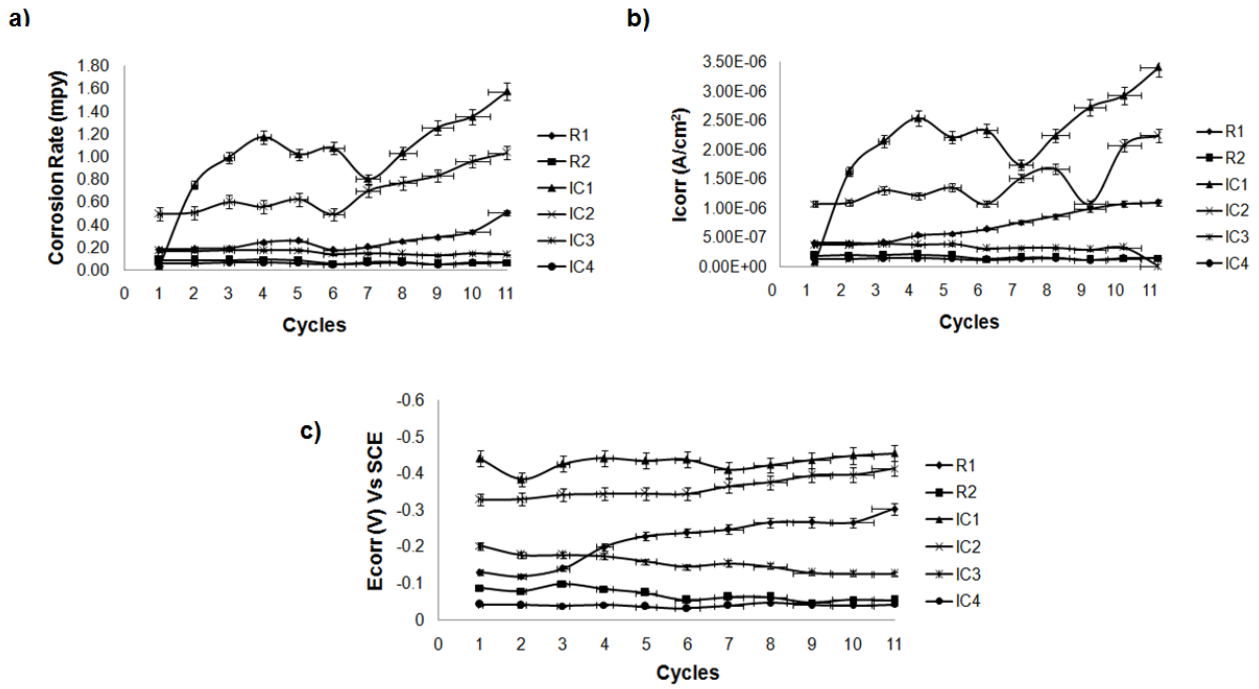

Figure 8. Electrochemical analysis of the reinforced concretes calculated by linear polarization resistance (LPR) method. (a) Corrosion rate, (b) Corrosion current (I_{corr}), (c) Corrosion potential (E_{corr}).

The corrosion rate of the concretes is illustrated in Figure 8(a). The IC1 and IC2 concretes exhibited the highest corrosion rates, followed by R1, with values of 1.58 mpy, 1.09 mpy, and 0.50 mpy, respectively. Lower corrosion rates were registered for the R2, IC3, and IC4 concretes. In the case of R2 concretes (0.06 mpy), the low corrosion rate can be attributed to the densification of the

cementitious matrix, since it contains PFA in substitution for OPC. The IC3 and IC4 concretes registered the lowest corrosion rates with 0.13 mpy and 0.06 mpy, respectively. This behavior can be attributed to the increased pore solution viscosity due to the use of SRA, which result in lower chloride ion migration through the concrete to the reinforced steel. In addition, the results agree with those obtained from the electrochemical permeability and chloride diffusion tests. From these results, it is confirmed that the concretes with the most suitable properties against corrosion are those made with the use of the internal curing technique and the addition of SRA.

Figure 8(b) corresponds to the evolution of I_{corr}, where it can clearly be seen that there is a similar behavior to that observed during the corrosion rate analysis. The concretes with the higher corrosion rates were found to be the R1, IC1, and IC2 concretes with values ranging from 1 x 10^{-6} A/cm^2 to 3.5 x 10^{-6} A/cm^2. The R2, IC3, and IC4 concretes exhibited lower corrosion rates with values below 5 x 10^{-7} A/cm^2. This behavior was constant during all the analyzed cycles. Once again, this behavior responds to a higher densification in the cementitious matrix via internal curing and the use of SRA additives, leading to lower chloride ion permeability. According to the criteria for estimating the corrosion of steel bar [96], the rebar is in a passive condition when I_{corr}<0.1 μA/cm^2; the corrosion extent of steel bar is low to moderate. When 0.1<I_{corr}<0.5 μA/cm^2; the corrosion extent of steel bar is moderate to high when 0.5<I_{corr}<1.0 μA/cm^2; the corrosion extent of steel bar is high when I_{corr}>1.0 μA/cm^2 [97]. Therefore, considering the value of corrosion rate in R2, IC3, and IC4 concretes, the steel bar is in low to moderate state, while the corrosion rate of steel bar in R1, IC1 and IC2 concretes is in high state.

From the E_{corr} analysis in Figure 8(c), it was found that the IC1 and IC2 concretes show the highest potential during the first analyzed cycles. As the cycles advanced, the R1 concrete showed a similar tendency as IC1 and IC2, where its corrosion resistance diminished with values above -0.3 V vs. SCE. The R2, IC3, and IC4 concretes showed a better behavior with values from -0.2 V to -0.05 V vs. SCE during all cycles. It is important to mention that the R2 and IC4 concretes contain PFA, an important parameter to be considered in the electrochemical behavior since increasing the content of PFA in the concrete results in a higher resistivity. The ASTM C876 standard [98] has determined three E_{corr} levels to identify the corrosion probability of steel bar in concrete. That is, when E_{corr} (vs SCE)>−0.20 V, the corroded probability of steel bar in concrete is less than 10%; when E_{corr} (vs SCE)<−0.35 V, the corroded probability of steel bar in concrete is more than 90%; when it locates in the middle region, the probability is uncertain. Therefore, R1, IC1, and IC2 concretes are in the middle region, i.e. the corroded probability is uncertain, while for R2, IC3, and IC4 concretes, the corroded probability of steel bar is less than 10%.

Finally, the corrosion resistance of steel bar in internal cured concretes is attributed to a reduction of the porosity in the cementitious matrix due to an improved hydration, i.e. the interface zone between steel and concrete is densified avoiding the ingress of deleterious agents resulting from chloride permeation and carbonation process [75]. Therefore, the electrochemical polarization resistance technique enables the corrosion mechanisms to be monitored and therefore allows for an acceptable determination of the damage in the reinforced steel, thereby intrinsically determining what type of concrete provides a higher durability.

4. CONCLUSIONS

The IC1 concrete registered the highest compressive resistance due to an internal curing effect since this concrete contains porous LWA that allows moisture transfer from the aggregates to the cement paste via a porous network, stimulating a hydration reaction with sufficient aging. In addition, the concretes based on the internal curing technology show a lower elastic modulus range than the conventional concretes. These mechanical property tendencies can be attributed to low porosity caused by the internal curing, leading to higher densification of the cementitious matrix, and the reduced density of the LWA in comparison to normal weight sand.

The IC2 and IC3 concretes obtained the lowest water absorption after 90 d of curing, which reduces harmful agent infiltration. The concretes that showed better results in the rapid chloride permeability tests were IC4, IC2, and R1. In the case of IC4 and IC2, a synergic effect of LWA and SRA provides good hydration, leading to densification of the cementitious matrix and a pore viscosity increment that improves the permeation properties. The usage of LWA and SRA additions in the concretes, influences the reduction of chloride ion diffusivity in the range of 60 % to 40 % in comparison to conventional concretes. The carbonation depth was also lower in the IC2 and IC3 concretes. The reported values of the LPR tests show that R2, IC3, and IC4 are above -0.1 V, which corresponds to a passive corrosion state.

The corrosion rate tests showed a lower value for the IC3 and IC4 concretes. These results agree with the results obtained in the permeability and chloride diffusion tests. The evolution of I_{corr} showed a similar behavior as that observed during the corrosion rate analysis. The IC3 and IC4 concretes exhibited lower corrosion rates with values below 5×10^{-7} A/cm^2. The E_{corr} of IC3 and IC4 indicated a more stable behavior with values from -0.2 V to -0.05 V vs. SCE.

As was observed, the synergic effect of LWA with SRA in the internal curing technology is efficient in prolonging the service life of reinforced concrete structures.

Pre-soaking the LWA in the SRA solution provided the best overall performance with respect to mechanical and transport properties in both concretes with and without fly ash substitution for cement. That is, IC4 performed in a superior manner when compared to R2 and IC3 outperformed R1, IC1, and IC2. This dual approach both increases the pore solution viscosity (SRA effect) and densifies the microstructure via enhanced hydration and a superior interfacial transition zone microstructure (IC/LWA effect).

ACKNOWLEDGMENTS

The first author thanks, National Technology Council of Mexico (CONACYT) by its support to accomplish their Master of Science studies, with the scholarship number 305954. Also, to the Universidad Autónoma de Nuevo León (UANL) by the supply of analytical equipment. It is also thanks the concrete technology department and the academic building materials group of Civil Engineering Faculty of the UANL. Special acknowledgments to Dr. Jose Manuel Mendoza Rangel for the discussion of the results.

References

1. A. Duran-Herrera, J.M. Mendoza-Rangel, E.U. De-Los-Santos, F. Vazquez, P. Valdez and D.P. Bentz, *Mater. Struct.*, 48 (4) (2015) 1207.
2. J.M. Mendoza-Rangel, J.M. Flores-Jarquín, E.U. De Los Santos and P. Garcés Terradillos, *Revista ALCONPAT.*, 6 (1) (2016) 41.
3. P. Lura, O.M. Jensen and S. Igarashi, *Mater.Struct.*, 40 (2007) 211.
4. S. Zhutovsky, K. Kovler and A. Bentur, *Cem. Concr. Comp.*, 26 (5) (2004) 499.
5. J. Zhang, Y. Dong Han and Y. Luosun, *J. Adv.Concr. Tech.*, 12 (2014) 456.
6. S. Zhutovsky, K. Kovler and A. Bentur, *Mater.Struct.*, 35 (2002) 97.
7. O.M. Jensen and P. Lura, *Mater.Struct.* 39 (2006) 817.
8. D.P. Bentz, J.M. Davis, M.A. Peltz and K.A. Snyder, *Mater.Struct*., 47 (2014) 581.
9. R. Henkensiefken, D. Bentz, T. Nantung and J. Weiss, *Cem. Concr. Comp.*, 31 (2009) 427.
10. M. Sahmaran, M. Lachemi, K.M.A. Hossain and V.C. Li, *Cem. Concr. Res*., 39 (2009) 893.
11. S. Weber and H. W. Reinhardt, *Adv. Cem. Bas. Mat.*, 6 (1997) 59.
12. A. Bentur, S. Igarashi and K. Kovler, *Cem. Concr. Res.*, 31(11) (2001) 1587.
13. P. Lura, D.P. Bentz, D.A. Lange, K. Kovler, A. Bentur and K.V. Breugel, *Mater.Struct.*, 39 (2006) 861.
14. C. Munteanu and M. Georgescu, *Rev. Rom. Mater.*, 42(2) (2012) 122.
15. D.P. Bentz, M.A. Peltz, K.A. Snyder and J. Davis, *Concr. Inter.*, 31 (2009) 31.
16. S. Zhutovsky and K. Kovler, *Cem. Concr. Res.*, 42(1) (2012) 20.
17. H. Ye, X. Jin, C. Fu, N. Jin, Y. Xu and T. Huang, *Constr. Build. Mater.*, 112 (2016) 457.
18. S.K. Verma, S.S. Bhadauria and S. Akhtar, *Rev. Rom. Mater.*, 45(3) (2015) 226.
19. C. Duran, *Constr. Build. Mater.*, 17 (2003) 147.
20. A. Paul and M. Lopez, *ACI Mater. J.*, 108(4) (2011) 385.
21. E. Sakai, K. Yamada, A. Ohta, *J. Adv. Concr. Tech.*, 1 (2003) 16.
22. E. Sakai, A. Ishida and A. Ohta, *J.Adv.Concr.Tech.*, 4 (2006) 221.
23. T. Sato, K. Goto and K. Sakai, *CAJ review of the 37th general meeting.*, (1983) 52.
24. C.K. Nmai, R. Tomita, F. Hondo and J. Buffenbarger, *Concr. Inter.*, (1998) 31.
25. K.J. Folliard and N.S. Berke, *Cem. Concr. Res.*, 27 (9) (1997) 1357.
26. M.S. Meddah and R. Sato, *ACI Mater. J.*, 107 (1) (2010) 65.
27. M.S. Meddah, M. Suzuki and R. Sato, *Constr. Build. Mater.*, 25 (2011) 239.
28. B. Rongbing and S. Jian, *Cem. Concr. Res.*, 35 (2005) 445.
29. D.P. Bentz. *Concr. Inter.*, 27 (10) (2005) 55.
30. D.P. Bentz, *J. Adv. Concr., Tech.* 4 (2006) 423.
31. I. Maruyama, K. Beppu, R. Kurihara and A. Furuta, *J. Adv. Concr. Tech.*, 14 (2016) 311.
32. A. Durán-Herrera, Pierre-Claude Aitcin and Nikola Petrov, *ACI Mater. J.*, 104 (1) (2007) 48.
33. A.A. Zaldívar-Cadena, I. Diaz-Peña, J.R. González-López, F. Vázquez-Acosta, A. Cruz-López, O. Vázquez-Cuchillo, F. Vázquez-Rodríguez and L.M. Serrato-Arias, *Adv. Mater. Res.*, 787 (2013) 286.
34. Z. Liu and W. Hansen, *K. Eng. Mater.*, 629 (2015) 201.
35. J. Justs, M. Wyrzykowski, D. Bajare and P. Lura, *Cem. Concr. Res.*, 76 (2015) 82.
36. D. Zou, H. Zhang, Y. Wang, J. Zhu, and X. Guan, *Constr. Build. Mater.*, 96 (2015) 209.
37. M. Kurt, M. S. Gül, R. Gül, A.C. Aydin and T. Kotan, *Constr. Build. Mater.*, 103 (2016) 36.
38. A. Terzic, L. Pezo, V. Mitic and Z. Radojevic, *Ceram. Inter.*, 41 (2015) 2714.
39. C. Ruiz-Santaquiteria, A. Fernández-Jiménez and A. Palomo, *Ceram. Inter.*, 41 (2015) 2714.
40. G. Rodriguez and A. Freitas, *Inter. J. Concr. Struct. Mater.*, 8 (3) (2014) 229.
41. J. Castro, L. Keiser, M. Golias and J. Weiss, *Cem. Concr. Comp.*, 33 (2011) 1001.
42. C. Schrofl, V. Mechtcherine, M. Gorges, *Cem. Concr. Res.*, 42 (2012) 865.
43. K. Onoue, H. Tamai, H. Suseno, *Constr. Build. Mater.*, 83 (2015) 261.

44. J. Zhang, J. Wang, Y. Han, *Constr. Build. Mater.*, 96 (2015) 599.
45. Y. Zhou, D. Deng, Z. Ng, T. Ji and X. Feng, *Constr. Build. Mater.*, 120 (2016) 373.
46. R. Liu, L. Jiang, J. Xu, C. Xiong and Z. Song, *Constr. Build. Mater.*, 56 (2014) 16.
47. Y. Hailong, J. Xianyu, F. Chuanqing, J. Nanguo, X. Yibin and H. Tao, *Constr. Build. Mater.*, 112 (2016) 457.
48. C. Chong, M. Cheung and B. Chan, *Corr. Sci.*, 69 (2013) 97.
49. S. Ahmad, *Cem. Concr. Comp.,* 25 (2003) 459.
50. S. Muthulingam and B.N. Rao, *Corr. Sci.*, 93 (2015) 267.
51. R. Vera, M. Villarreal, A.M. Carvajal, E. Vera and C. Ortiz, *Mater. Chem. Phys.*, 114 (2009) 467.
52. W. Yeih, J. Chang, *Constr. Build. Mater.*, 19 (2005) 516.
53. J. Xia, W. Jin and L. Li, *Corr. Sci.*, 53 (2011) 1794.
54. K. JeevaJothi and K. Palanivelu, *Ceram. Inter.*, 39 (7) (2013) 7619.
55. E. Medvedovski, *Ceram. Inter*., 39 (3) (2013) 2723.
56. F.J. Vázquez-Rodríguez, E.U. De los Santos, J.M. Mendoza-Rangel, C. Gómez-Rodríguez, A. Arato and Edén A. Rodríguez, *Rev. Rom. Mater.*, 47 (4) (2017) 505.
57. C. Andrade, V. Castelo, C. Alonso, J.A. Gonzalez, ASTM SP., 906 (1984) 43.
58. C. Andrade, C.L. Page, *Cem. Concr. Res.,* 21 (1986) 49.
59. J.A. Gonzalez, C. Andrade, C. Alonso and S. Feliu, *Cem. Concr. Res.,* 25 (1995) 257.
60. J.G. Cabrera, *Cem. Concr. Comp.,* 18 (1996) 47.
61. C. Alonso, C. Andrade, M. Castellote, P. Castro, *Cem. Concr. Res.,* 30 (2000) 1047.
62. H. Won. Song, V. Saraswathy*, Int. J. Electrochem. Sci.,* 2 (2007) 1.
63. D.M. Bastidas, A. Fernández-Jiménez, A. Palomo, J.A. González, *Corr. Sci.,* 50 (2008) 1058.
64. L. Abosrra, A.F. Ashour, M. Youseffi, *Constr. Build. Mater.,* 25 (2011) 3915.
65. R. Corral-Higuera, S.P. Arredondo-Rea, M.A. Neri-Flores, J.M. Gómez-Soberón, J.L. Almaral-Sánchez, J.H. Castorena-González, A. Martínez-Villafañe, F. Almeraya-Calderón, *Int. J. Electrochem. Sci.,* 6 (2011) 958.
66. D. Nieves-Mendoza, C. Gaona-Tiburcio, H.L. Hervert-Zamora, R. Tobias J, P. Castro-Borges, R. Colas O, P. Zambrano Robledo, Martínez-Villafañe A, F. Almeraya-Calderón, *Int. J. Electrochem. Sci*., 7 (2012) 5495.
67. R. Vera, R. Venegas, A.M. Carvajal, F. Corvo, T. Pérez, *Int. J. Electrochem. Sci.,* 7 (2012) 10722.
68. R. Puente-Ornelas, L.Y. Gómez-Zamorano, M.C. Alonso, P.C. Zambrano, A.M. Guzmán, E. Rodríguez, B. Bermúdez-Reyes, M. Sánchez-Moreno, *Int. J. Electrochem. Sci.,* 7 (2012) 136.
69. E.I. Moreno, R.G. Solís-Carcaño, J. Varela-Rivera, J.C. Pacho-Monforte, R.A. Cua-Cuevas, *Int. J. Electrochem. Sci.,* 10 (2015) 6444.
70. L.E. Narváez, R.I. Rosales-Martínez, L. Narváez-Hernández, L.S. Hernández- Hernández, J.M. Miranda-Vidales, *Int. J. Electrochem. Sci.,* 10 (2015)10003.
71. M.J. Pellegrini-Cervantes, C.P. Barrios-Durstewitz, R.E. Nuñez-Jaquez, S.P. Arredondo-Rea, F.J. Baldenebro-Lopez, M. Rodríguez- Rodríguez, L.G. Ceballos-Mendivil, A. Castro-Beltrán, G. Fajardo-San-Miguel, F. Almeraya-Calderon, A. Martinez-Villafañe, *Int. J. Electrochem. Sci*., 10 (2015) 332.
72. W. Aperador, A. Delgado, J. Bautista-Ruiz, *Int. J. Electrochem. Sci.,* 11 (2016) 2297.
73. A.M. Aguirre-Guerrero, R. Mejía-de-Gutiérrez, M.J. Ribeiro Montês-Correia, *Constr. Build. Mater.,* 121 (2016) 704.
74. M.I. Allan, B.W. Cherry, *J. Corros. Eng.,* (1992) 426.
75. Y. Liu, R.E. Weyers, *ACI Mater J.,* 95(6) (1998) 675.
76. D. Cusson, Z. Lounis, L. Daigle, *Cem. Concr. Comp.,* 32 (2010) 339.
77. R. Francois, G. Arliguie, *J. Mater. Civ. Eng.,* 10 (1) (1998) 14.
78. ASTM C618–08 Standard Specification for Coal Fly Ash and Raw or Calcined Natural Pozzolan for use as a Mineral Admixture in Concrete, Annual Book of ASTM Standard., 2000.

79. ASTM C138/C138M-16a Standard Test Method for Density (Unit Weight), Yield, and Air Content (Gravimetric) of Concrete, Annual Book of ASTM Standard., 2016.
80. ASTM C143/C143M-15a Standard Test Method for Slump of Hydraulic-Cement Concrete, Annual Book of ASTM Standard., 2015.
81. ASTM C173/C173M-16 Standard Test Method for Air Content of Freshly Mixed Concrete by the Volumetric Method, Annual Book of ASTM Standard., 2016.
82. ASTM A370-17 Standard Test Methods and Definitions for Mechanical Testing of Steel Products, Annual Book of ASTM Standard., 2017.
83. ASMT C39-16b Standard Test Method for Compressive Strength of Cylindrical Concrete Samples, Annual Book of ASTM Standard., 2016.
84. ASTM C469-14 Standard Test Method for Static Modulus of Elasticity and Poisson's Ratio of Concrete in Compression. Annual Book of ASTM Standard., 2014.
85. ASTM C642-13 Standard Test Method for Density, Absorption, and Voids in Hardened Concrete, Annual Book of ASTM Standard., 2013.
86. ASTM C1202-12 Standard Test Method for Electrical Indication of Concrete's Ability to Resist Chloride Ion Penetration, Annual Book of ASTM Standard., 2012.
87. ASTM C1556-11a Standard Test Method for Determining the Apparent Chloride Diffusion Coefficient of Cementitious Mixtures by Bulk Diffusion, Annual Book of ASTM Standard., 2016.
88. F.U.A. Shaikh, S.W.M. Supit, *Constr. Build. Mater*., 99 (2015) 208.
89. F.U.A. Shaikh, S.W.M. Supit, *Constr. Build. Mater*., 82 (2015) 192.
90. M. Stern and A.L. Geary, *J. Electrochem. Soc.*, 104 (1) (1957) 56.
91. V. S. Sastri, E. Ghali and M. Elboujdaini, Corrosion Prevention and Protection Practical Solutions, John Wiley & Sons, England (2007)
92. Pine Research Instrumentation, Linear Polarization resistance and corrosion rate, datasheet, Rev.002 (2016)
93. H.K. Kim, J.G. Jang, Y.C. Choi, H.K. Lee, *Constr. Build. Mater.*, 71(2014) 339.
94. D.P. Bentz, P.E. Stutzman and B. Mohr, *ACI SP*-256 (2008) 81.
95. D.P. Bentz, K.A. Snyder, M.A. Peltz, K. Obla, and H. Kim, *ACI Mater. J.*, 110(5) (2013) 495.
96. S.G. Millard, K.R. Gowers and Js. Gill, *ACI SP-128* (1991) 373.
97. J. Wei, X.X. Fu, J.H. Dong and W. Ke, *J. Mater. Sci Technol.*, 28(10) (2012) 905.
98. ASTM C876-15 (2015) Standard test method for half-cell potentials of uncoated reinforcing steel in concrete. Annual Book of ASTM Standard., 2015.